Development of transition edge sensor detectors optimized for single-photon spectroscopy in the optical and near-infrared

Peter C. Nagler[a], Matthew A. Greenhouse[a], S. Harvey Moseley[a], Bernard J. Rauscher[a], and John E. Sadleir[a]

[a]NASA/Goddard Space Flight Center, Greenbelt, MD USA

ABSTRACT

The search for biosignatures in the atmospheres of exoplanets will be a key focus of future space telescopes that operate in the ultraviolet, visible, and near-infrared bands. Detection of biosignatures requires an instrument with moderate spectral resolving power ($R \sim 100$) and a large bandwidth (~ 400 nm – ~ 1.8 μm). Additionally, biosignature detection is a photon-starved science; instruments designed for these measurements would ideally combine high optical efficiency with quantum-limited photon detectors (i.e., detectors that exhibit zero dark current). In this work, we report on our efforts to develop energy resolving transition edge sensor (TES)-based detectors designed for biosignature detection. TESs operated as microcalorimeters are compelling detectors for this application. Unlike semiconductor detectors, TESs eliminate the need for dispersive optics and are truly single photon detectors – fundamental TES noise yields uncertainty in the energies of detected photons, not in the number of detected photons. We introduce TESs designed for this application and discuss the path toward realizing a TES-based dispersionless spectrometer optimized for biosignature detection.

Keywords: biosignature detection, single photon detectors, transition edge sensors, imaging spectroscopy

1. INTRODUCTION

The search for life on other worlds holds pride of place in NASA's 30-year strategic vision for astrophysics.[3,4] Already, concepts exist for a Large Ultraviolet-Optical-Infrared (LUVOIR) space telescope equipped with a coronagraph and a starshade-based Habitable ExoPlanet Imaging Mission (HabEx).[5] For either concept, once a promising "exoEarth" candidate is found, spectroscopic biosignature characterization (Figure 1) will be used to seek evidence of life.

Unfortunately, even with 12 meters of aperture, biosignature characterization is extremely photon starved. For example, assuming a solar twin at 15 pc and an Earth-twin seen at quadrature, the count rate is only ~ 0.006 ph s^{-1} pix^{-1} at 760 nm in the focal plane of a dispersed coronagraph.[6,7] This feeble flux includes contributions from the exoEarth, Zodiacal and extra-Zodiacal light, and assumes a coronagraph background that is dominated by these astronomical sources. With a source arrival rate (excluding backgrounds) of only about one photon every 6 minutes per pixel in a dispersed focal plane, a noiseless detector – i.e., a nearly quantum-limited single photon detector – is highly desirable.

In this work, we discuss the use of a transition edge sensor (TES) operated as a microcalorimeter for biosignature detection. TESs are especially attractive biosignature detector candidates. In contrast to semiconductor detectors, TESs have no read noise (in the traditional astronomy sense) and no dark current. TESs are energy resolving, enabling non-dispersive imaging spectroscopy at sufficient resolving powers for biosignature detection. In Section 2, we provide a brief review of semiconductor single photon detectors and introduce low temperature detectors as an alternative. In Section 3, we discuss the unique potential of a TES as a biosignature detector, especially noting the recent advances in signal processing that will enable a TES to meet the requirements imposed by biosignature detection. We show results of calculations that apply results of non-linear signal processing to realistic LUVOIR-type devices. Finally, in Section 4, we discuss ongoing work toward building and testing a biosignature detection-capable TES.

Further author information: Send correspondence to Jack Sadleir
E-mail: john.e.sadleir@nasa.gov, Telephone: 1-301-286-3078

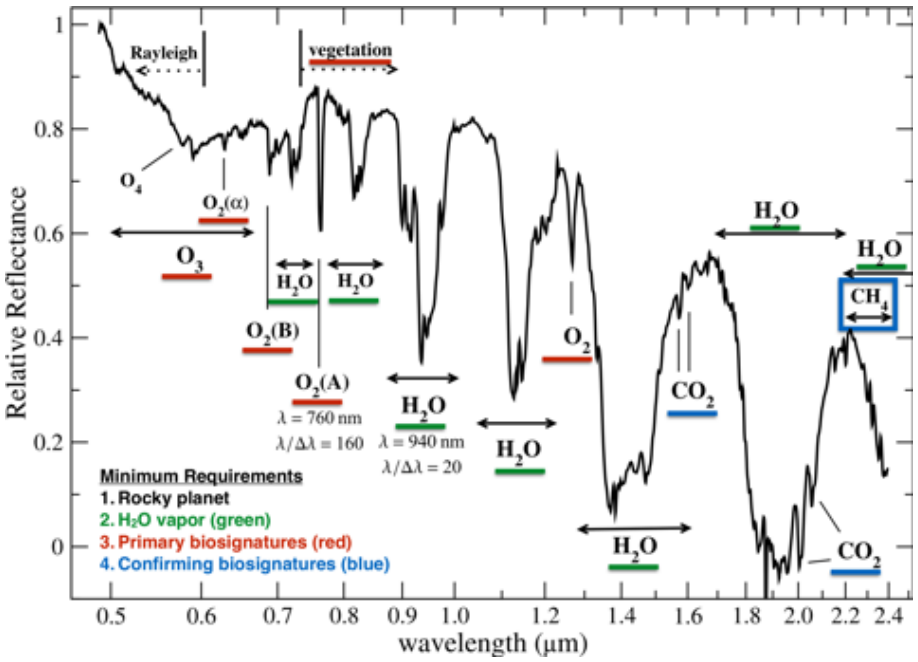

Figure 1. The Earth seen as an exoplanet, adapted from Turnbull *et al.*[1] To make the spectrum, Turnbull *et al.*[1] observed the Earth, as reflected back by the night side of the moon. Biosignatures are atmospheric features that indicate potential life. Once a rocky planet is found, H_2O is necessary for life as we know it. Biological processes can make O_2 and O_3, although abiotic mechanisms (e.g., photo-dissociation of H_2O) are possible. Confirming biosignatures[2] are needed to rule out false positives. H_2O at $\lambda = 940$ nm and O_2 at $\lambda = 760$ nm are particularly important biosignatures. The 760 nm O_2 line sets the nominal requirement for resolving power, $R = \lambda/\Delta\lambda > 100$.

2. SINGLE PHOTON DETECTORS

A true single photon detector is nearly quantum-limited. Compared to other instrumental sources of noise, a single photon detector would contribute negligible uncertainty to the number of measured photons. Although several semiconductor-based "photon counting" detector technologies exist (e.g., *e2v*'s electron multiplying CCD (EMCCD)[8]), all semiconductor detectors add noise. This noise manifests itself as false positive or "dark" counts (where a photon is counted, but no photon actually arrived).

There are unavoidable practical reasons for this. All real semiconductors have imperfections, and some of these will manifest as electrically active defect states (charge "traps") in the bandgap. For typical $T \geq 80$ K visible and infrared (VISIR) detector operating temperatures, there will always be sufficient thermal energy in the semiconductor to promote some charges across the bandgap with the assistance of traps to appear as dark current. Even if one could make a perfectly defect-free crystal, once in space, proton irradiation would create defects.[9] Moreover, charge traps can manifest in other undesirable ways besides dark current; the charge transfer inefficiency degradation in n-channel CCDs, including EMCCDs, is caused by trapping.

In contrast to detectors sensitive to single electron energetics and localized defect states, the TES is a thermodynamic detector. The signal is a thermodynamic quantity (the temperature of the electron system in a solid) – the average of a very large system. A dark count event for the TES would occur if a noise record were mistaken for a thermal pulse. If we just recorded dark noise traces, and assuming typical sampling rates with a resolving power $R \sim 4$, a TES would give only one dark count – a false-positive in-band photon – per age of the universe. Another type of false positive occurs when two photons arrive at a pixel within a small time window. For the ExoEarth about 1 in every billion photons will fall within ± 5 ns of each other; these very rare events can be rejected with negligible impact on the absorption efficiency. TESs are immune to local defects. They are composed of standard-coupling elemental BCS superconductors that have very large characteristic lengths ($\sim$ 10s of nm) that become significantly larger still very near the transition temperature T_c. For such

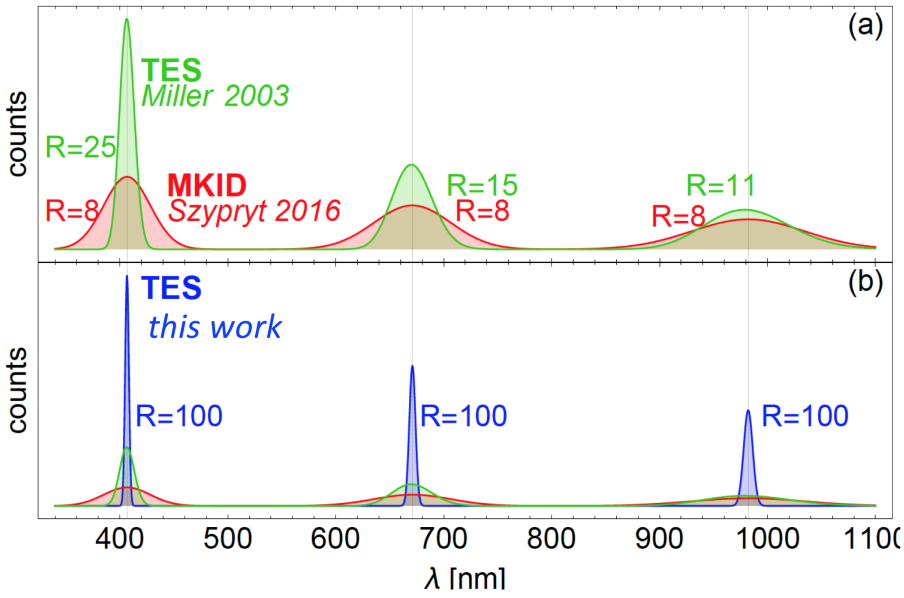

T

Figure 2. Built-in energy resolution line profiles of: (a) existing MKID and linear TES detector, (b) predicted response for a non-linear TES with resolving power $R = 100$. The line profiles show each respective detector's response to the same number of photons at three wavelengths: $\lambda = 406.6$ nm, 671 nm, and 982.1 nm. We show these photon energies because they represent published test data for the existing MKIDs and linear TESs.[16,17]

superconductors, the energy gap and T_c are insensitive to nonmagnetic impurities and crystallographic defects (Anderson's theorem).[10]

TESs have operated as single photon detectors in the ultraviolet (UV), optical and near-infrared (NIR) bands for decades. For astrophysics applications, small format TES arrays developed by Cabrera *et al.* have achieved better resolving power than any other single photon detector (Figure 2),[11–15] and they can also provide sub-μs timing (photon arrival) information. Deployed from the ground, the detectors achieved a resolving power $E/\Delta E_{\mathrm{FWHM}} \simeq 20$ at 400 nm during phase-resolved spectrophotometric observations of the Crab pulsar.[12–14] In these observations maximum accessible energy was limited to ~ 3 eV, however in laboratory calibration the TESs exhibited uniform energy sensitivity from 0.3 eV to > 10 eV.[13]

More recently, optical TES detectors have been successfully used for applications in quantum optics and quantum information science. These fields require a detector exhibiting extremely high detection efficiency, no dark counts, high count rates, and sufficient spectral resolution to resolve the number of incident monochromatic photons stemming from quantum optical processes. The TES energy resolution demonstrated by Cabrera *et al.* in 1998[11] is suffucient for these applications, so the most recent optical TES work has focused on achieving the highest optical efficiency possible (now routinely in excess of ninety percent for fiber-coupled devices[18]) and speeding up devices to accommodate high count rates. The latter is accomplished by raising the device's operating temperature, trading energy resolution (already sufficiently high) for speed.[19] These efforts to increase speed and efficiency recently led to the first demonstrations of a loophole-free test of Bell's inequality, a long-sought goal in experimental quantum physics.[20]

Although other single photon low temperature detectors (LTDs) exist, including microwave kinetic inductance detectors (MKID), Superconducting Nanowire Single Photon Detectors (SNSPD), and Superconducting Tunnel Junction (STJ) arrays, TESs are uniquely promising in the context of biosignature detection. Compared to MKIDs, TESs have already demonstrated better spectral resolution in the optical and NIR and we believe that TESs show unique promise to meet biosignature characterization's $R = \lambda/\Delta\lambda > 100$ spectral energy resolving requirement (see Figure 2). In contrast to SNSPDs, TESs are energy resolving.

Individual STJ detectors have achieved $R \sim 7$,[21] but their use in astrophysics has been limited by the lack of an effective multiplexing system and the difficulty of optimizing STJs for efficient optical absorption over a wide

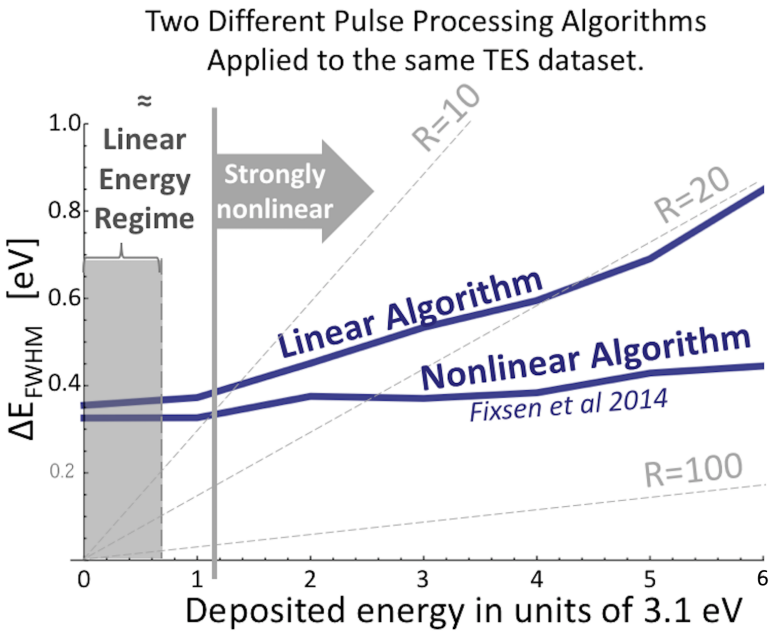

T

Figure 3. Comparison of linear and non-linear pulse processing algorithms, adapted from Fixsen *et al.*[25] The non-linear algorithm gives near-constant $\Delta E_{\rm FWHM}$ out to the largest photon energies measured. Gray dashed lines are contours of constant resolving power. Standard TES spectrometer design would be limited to photon energies in the shaded gray Linear Energy Regime.

wavelength range. In contrast, TES spectrometers can apply the full range of multiplexing systems developed for x-ray and cosmic microwave background (CMB) applications. For example, the LYNX x-ray mission under study for the 2020 decadal survey is developing a SQUID-based readout system for a focal plane consisting $\sim 10^5$ TES microcalorimeters, larger than the nominal $\sim 241 \times 241$ array needed for LUVOIR. CMB experiments (e.g., SPIDER,[22] BICEP/KECK,[23] EBEX[24]) regularly deploy focal planes with thousands of multiplexed TESs.

3. THE TES AS A BIOSIGNATURE DETECTOR

In this section, we describe the path toward realizing a biosignature-detecting TES. We start with a review of the thermodynamics of a TES and the TES design considerations typically employed for a given spectroscopy application. Then we discuss a non-linear pulse processing algorithm recently developed at NASA/GSFC that greatly expands the parameter space over which a given device can operate. We present modeling results that show how a TES designed with the standard thermodynamic model can meet the requirements of a LUVOIR or HABEX-type mission by operating in the non-linear regime.

3.1 Thermodynamic TES Model

The laws of thermodynamics, applied to any physical system with dissipation, require associated fluctuations in its state variables (noise). For a TES, the known thermodynamic fluctuations are associated with electrical resistance (Johnson noise in the TES resistance R_0 and in the bias shunt resistor $R_{\rm sh}$) and thermal impedance (phonon noise or thermal fluctuation noise (TFN) across the thermal link G that connects the sensor to the bath). These noise sources set a fundamental thermodynamic limit on the achievable energy resolution $\Delta E_{\rm FWHM}$ of a TES. The expression for $\Delta E_{\rm FWHM}$, the energy uncertainty due to thermodynamic noise, simplifies to a compact form[26] if we assume negligible amplifier noise, negligible shunt resistor Johnson noise, and large loop gain:

$$\Delta E_{\rm FWHM} = 2\sqrt{2\log 2}\sqrt{\frac{4k_B T_0^2 C\sqrt{n/2}}{\sqrt{1-(T_b/T_0)^n}}}\sqrt{\frac{1+2\beta}{\alpha^2}}. \quad (1)$$

Here T_0 and T_b are the temperature of the TES and bath respectively, n is a thermal exponent describing the power from through the thermal link G ($n \simeq 5$ for electron-phonon conductance), C is the total heat capacity, and α and β are both dimensionless parameters characterizing the sensitivity of the resistive transition to changes in temperature and current respectively, and α and β are defined as the logarithmic derivative of the resistance with respect to temperature and current, respectively: $\alpha = (T_0/R_0) \times (\delta R/\delta T)$ and $\beta = (J_0/R_0) \times (\delta R/\delta J)$. The expression simplifies further in the limit $\beta \to 0$ and $T_b << T_0$ to

$$\Delta E_{\mathrm{FWHM}} = 2\sqrt{2\log 2}\sqrt{4k_B T_0^2 \frac{C}{\alpha}\sqrt{n/2}}. \tag{2}$$

From Equation 2, we can reduce ΔE_{FWHM} (thereby increasing sensitivity) by reducing the temperature, reducing the heat capacity, and increasing α. Such changes increase the detector's responsivity and for a linear device increase the pulse height (PH) of the current pulse $|\delta J\,(t)|$ for the same photon energy. But the high-sensitivity part of the resistive transition exists only over a finite temperature range and the detector "saturates" for photon energies greater than $E_{\mathrm{sat}} = CT_0/\alpha$. Designing TESs to stay in the linear regime, combined with the finite temperature range of high sensitivity in the resistive transition, forces a tradeoff between the spectral range and the energy resolution.

To illustrate this tradeoff, we define the minimum and maximum photon energies in band of interest to be $E_{\gamma\mathrm{min}}$ and $E_{\gamma\mathrm{max}}$, respectively. It is useful to define a unitless saturation factor $SatFactor$, defined as the ratio between a given photon's energy and the detector's saturation energy: $SatFactor = E_\gamma/E_{\mathrm{sat}}$. The saturation factor measures how close to (or beyond) saturation the TES is for a particular incident photon energy. The general approach for TES spectroscopy applications is to design the TES to operate within the linear regime over the entire photon energy band of interest. This means the devices are designed with the *requirement* that $SatFactor < 1$ for photon energies up to $E_{\gamma\mathrm{max}}$. Then a linear optimal filter can then be applied to each measured current pulse event to extract the photon's energy. From Equation 2, this approach sets an upper limit on TES temperature T_0 for a specific spectroscopy application. The standard design practice is to work with this T_0 value (typically $\alpha \sim 50$ to 1000 or more) and design the total heat capacity C so that the device nears saturation at the highest photon energy of interest. Applying this method to LUVOIR-like requirements, with $0.69\,\mathrm{eV} < E_\gamma < 3.1\,\mathrm{eV}$ and $E_\gamma/\Delta E_{\mathrm{FWHM}} \geq 100$, we find that the TES temperature T_0 must be 5 mK or less for realistic device geometries and materials (Figure 4).

3.2 Non-linear TES operation

Many restrictions encountered in standard TES design can be lifted if a device can operate in the non-linear regime, where $SatFactor > 1$. There is significant evidence that this is a viable solution that greatly expands the parameter space over which a TES can operate. Compared to linear operation, non-linear operation enables combinations of higher resolving powers, over broader bands, at higher operating temperatures.

Work by Fixsen *et al.*[25] (Figure 3) compares the standard linear optimal filter technique with the non-linear algorithm developed at NASA/GSFC for a dataset with non-linear TES pulse records at photon energies from 3 eV to 18 eV. The device under test was a NIST/Boulder-developed W TES designed for quantum communications applications at $\lambda = 1550$ nm (0.8 eV). The nonlinear algorithm gives improved energy resolution at all energies measured. For the largest photon energy measured, the standard linear technique's ΔE_{FWHM} increased by a factor of 2.4. The non-linear algorithm gives near-constant ΔE_{FWHM} from the small signal value up to the largest energies measured at $SatFactor = 8$.

Busch *et al.*[28] achieved similar results. Data were on a MoAu TES taken using Al Kα (1.5 keV) and Mn Kα (5.9 keV) x-ray sources. The device was linear at 1.5 keV and non-linear at 5.9 keV. The resolving power achieved with the non-linear algorithm for 5.9 keV data was better than the resolving power achieved with a standard optimal filter for 1.5 keV data, giving $R \sim 3200$ and $R \sim 1800$, respectively. Again we find the nonlinear algorithm improved the energy resolution out to the largest energies measured.

Assuming a realistic device designed to meet required energy resolution in the linear regime, we modeled the relationship between operating temperature, resolving power, and $SatFactor$. The results are shown in Figures 4 and 5. Figure 4 shows the tradeoff between TES operating temperature and $SatFactor$. It illustrates that

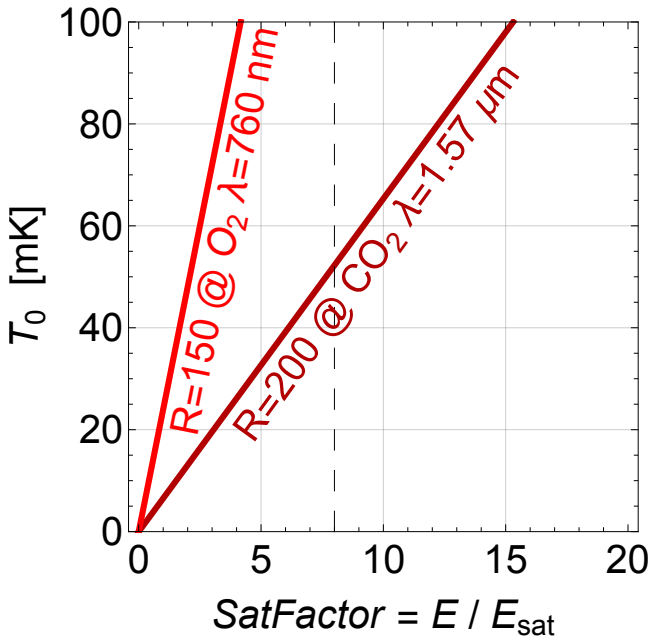

T

Figure 4. Illustration of the trade off between operating temperature T_0 and non-linearity ($SatFactor$) for two important biosignature lines and resolving power R goals. The vertical dashed line is the most non-linear TES measurement, where $\Delta E_{\rm FWHM}$ is flat out to $SatFactor = 8$. Recognize that to satisfy $R = 200$ at $\lambda = 1.57$ μm we can run the TES just as non-linear as Fixsen *et al.* at a temperature of 53 mK, or we can increase the $SatFactor$ (more non-linear) and operate at a higher temperature. Until this point, TESs have been designed to operate in the linear regime, where $SatFactor < 1$. Compared to a linear TES, operating in the non-linear regime enables significantly higher energy sensitivities for the same temperature.

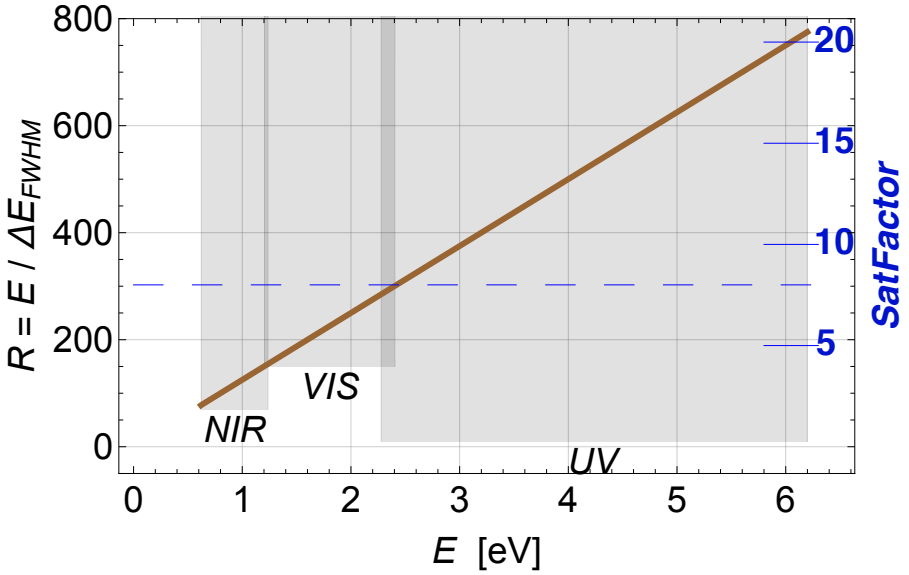

T

Figure 5. Left: R vs. E (brown) for a non-linear TES with $\Delta E_{\rm FWHM} = 8$ meV. The shaded gray regions show each band considered for *LUVOIR* and its nominal R requirement (NIR: $R \geq 70$, VIS: $R \geq 150$, UV: $R \geq 10$).[27] The device achieves $R = 203$ at 760 nm (O_2 line) and $R = 98$ at 1570 nm (CO_2 line). This TES operates at 70 mK and covers the entire NIR and VIS bands requiring no more non-linearity than already demonstrated by Fixsen *et al.*[25] With a larger $SatFactor$, we can either decrease $\Delta E_{\rm FWHM}$ or increase the TES operating temperature T_0.

increasing the $SatFactor$ means the TES can be operated at higher temperatures. The CO_2 line at 1.57 μm can be resolved at $R = 200$ at a $SatFactor$ that has already been demonstrated experimentally and at temperatures accessible to space-qualified cryostats. Achieving $R = 150$ at the 760 nm O_2 line requires even less saturation. Figure 5 demonstrates how a device operating at 70 mK can meet nominal LUVOIR requirements with the same non-linearity as the devices tested by Fixsen *et al.*[25]

4. CONCLUSIONS

The TES is a compelling candidate as a biosignature detector. It has no dark current and read noise (in the conventional astronomy sense), and it eliminates the need for a dispersive spectrometer. TESs are nearly quantum-limited detectors. As such, the uncertainty in number of collected photons is expected to be dominated by other instrument systematics (such as scattered light) and/or environmental disturbances of the TESs. Already TESs have demonstrated better energy resolving power than any other energy-resolving single photon detector in the LUVOIR band, despite little recent development for astrophysics applications. Advances in coupling light to a TES means they can now operate with near-unity efficiency,[18] and a single broadband TES can satisfy biosignature detection requirements across the UV, optical, and NIR bands. Using the thermodynamic TES model (Section 3.1), we can design a device that meets biosignature detection requirements. For non-linear operation (Section 3.2), the device needs to meet the ΔE_{FWHM} requirement at the lowest energy of the band where $SatFactor < 1$, and then not degrade as $SatFactor$ increases. Up to the highest $SatFactor$ measured to date, there is no observed degradation of ΔE_{FWHM}. Compared to the best TES energy resolution result in the optical achieved by Miller *et al.*,[17] we will meet the ΔE_{FWHM} requirements by: 1) reducing thermal fluctuation noise by reducing the operating temperature from 125 mK to 70 mK or lower; 2) reducing the heat capacity by reducing the TES volume or choosing a sensor material with fewer carriers; 3) reducing athermal phonon losses by building devices on a membrane or otherwise isolated substrate; 4) reducing hot quasiparticle losses by choosing a higher-T_c lead material. We are currently in the process of building and testing devices that address each of these changes. Beyond adjusting each available parameter in the thermodynamic TES model, we will also explore device behavior under extreme saturation ($SatFactor > 8$).

REFERENCES

[1] Turnbull, M. C., Traub, W. A., Jucks, K. W., Woolf, N. J., Meyer, M. R., Gorlova, N., Skrutskie, M. F., and Wilson, J. C., "Spectrum of a Habitable World: Earthshine in the Near-Infrared," *ApJ* **644**, 551–559 (June 2006).

[2] Schwieterman, E. W., Meadows, V. S., Domagal-Goldman, S. D., Deming, D., Arney, G. N., Luger, R., Harman, C. E., Misra, A., and Barnes, R., "Identifying Planetary Biosignature Impostors: Spectral Features of CO and O_4 Resulting from Abiotic O_2/O_3 Production," *ApJ* **819**, L13 (Mar. 2016).

[3] Kouveliotou, C., Agol, E., Batalha, N., Bean, J., Bentz, M., Cornish, N., Dressler, A., Figueroa-Feliciano, E., Gaudi, S., Guyon, O., Hartmann, D., Kalirai, J., Niemack, M., Ozel, F., Reynolds, C., Roberge, A., Straughn, K. S. A., Weinberg, D., and Zmuidzinas, J., "Enduring Quests-Daring Visions (NASA Astrophysics in the Next Three Decades)," *ArXiv e-prints* (Jan. 2014).

[4] Dalcanton, J., Seager, S., Aigrain, S., Battel, S., Brandt, N., Conroy, C., Feinberg, L., Gezari, S., Guyon, O., Harris, W., Hirata, C., Mather, J., Postman, M., Redding, D., Schiminovich, D., Stahl, H. P., and Tumlinson, J., "From Cosmic Birth to Living Earths: The Future of UVOIR Space Astronomy," *ArXiv e-prints* (July 2015).

[5] Mennesson, B., Gaudi, S., Seager, S., Cahoy, K., Domagal-Goldman, S., Feinberg, L., Guyon, O., Kasdin, J., Marois, C., Mawet, D., Tamura, M., Mouillet, D., Prusti, T., Quirrenbach, A., Robinson, T., Rogers, L., Scowen, P., Somerville, R., Stapelfeldt, K., Stern, D., Still, M., Turnbull, M., Booth, J., Kiessling, A., Kuan, G., and Warfield, K., "The Habitable Exoplanet (HabEx) Imaging Mission: preliminary science drivers and technical requirements," in [*Space Telescopes and Instrumentation 2016: Optical, Infrared, and Millimeter Wave*], *Proc. SPIE* **9904**, 99040L (July 2016).

[6] Stark, C. C., Roberge, A., Mandell, A., Clampin, M., Domagal-Goldman, S. D., McElwain, M. W., and Stapelfeldt, K. R., "Lower Limits on Aperture Size for an ExoEarth Detecting Coronagraphic Mission," *ApJ* **808**, 149 (Aug. 2015).

[7] Stark, C. C. Private communication (2017).

[8] Teledyne-e2v. https://www.e2v.com/products/imaging/emccd-image-sensors-for-space-and-ground-based-astronomy/Online (2018).

[9] Harding, L. K., Demers, R. T., Hoenk, M., Peddada, P., Nemati, B., Cherng, M., Michaels, D., Neat, L. S., Loc, A., Bush, N., Hall, D., Murray, N., Gow, J., Burgon, R., Holland, A., Reinheimer, A., Jorden, P. R., and Jordan, D., "Technology advancement of the CCD201-20 EMCCD for the WFIRST coronagraph instrument: sensor characterization and radiation damage," *Journal of Astronomical Telescopes, Instruments, and Systems* **2**, 011007 (Jan. 2016).

[10] Anderson, P., "Theory of dirty superconductors," *Journal of Physics and Chemistry of Solids* **11**, 26–30 (Sept. 1959).

[11] Cabrera, B., Clarke, R. M., Colling, P., Miller, A. J., Nam, S., and Romani, R. W., "Detection of single infrared, optical, and ultraviolet photons using superconducting transition edge sensors," *Applied Physics Letters* **73**, 735 (Aug. 1998).

[12] Romani, R. W., Cabrera, B., Figueroa, E., Miller, A. J., and Nam, S. W., "TES Spectrophotometers: First Astronomical Observations and Future Potential," in [*American Astronomical Society Meeting Abstracts*], *Bulletin of the American Astronomical Society* **30**, 1266 (Dec. 1998).

[13] Romani, R. W., Miller, A. J., Cabrera, B., Figueroa-Feliciano, E., and Nam, S. W., "First Astronomical Application of a Cryogenic Transition Edge Sensor Spectrophotometer," *ApJ* **521**, L153–L156 (Aug. 1999).

[14] Romani, R. W., Miller, A. J., Cabrera, B., Nam, S. W., and Martinis, J. M., "Phase-resolved Crab Studies with a Cryogenic Transition-Edge Sensor Spectrophotometer," *ApJ* **563**, 221–228 (Dec. 2001).

[15] Burney, J., Bay, T. J., Barral, J., Brink, P. L., Cabrera, B., Castle, J. P., Miller, A. J., Nam, S., Rosenberg, D., Romani, R. W., and Tomada, A., "Transition-edge sensor arrays for UV-optical-IR astrophysics," *Nuclear Instruments and Methods in Physics Research A* **559**, 525–527 (Apr. 2006).

[16] Szypryt, P., Mazin, B. A., Ulbricht, G., Bumble, B., Meeker, S. R., Bockstiegel, C., and Walter, A. B., "High quality factor platinum silicide microwave kinetic inductance detectors," *Applied Physics Letters* **109**, 151102 (Oct. 2016).

[17] Miller, A. J., Nam, S. W., Martinis, J. M., and Sergienko, A. V., "Demonstration of a low-noise near-infrared photon counter with multiphoton discrimination," *Applied Physics Letters* **83**, 791 (July 2003).

[18] Lita, A. E., Miller, A. J., and Nam, S. W., "Counting near-infrared single-photons with 95% efficiency," *Optics Express* **16**, 3032 (2008).

[19] Lamas-Linares, A., Calkins, B., Tomlin, N. A., Gerrits, T., Lita, A. E., Beyer, J., Mirin, R. P., and Woo Nam, S., "Nanosecond-scale timing jitter for single photon detection in transition edge sensors," *Applied Physics Letters* **102**, 231117 (June 2013).

[20] Shalm, L. K., Meyer-Scott, E., Christensen, B. G., Bierhorst, P., Wayne, M. A., Stevens, M. J., Gerrits, T., Glancy, S., Hamel, D. R., Allman, M. S., Coakley, K. J., Dyer, S. D., Hodge, C., Lita, A. E., Verma, V. B., Lambrocco, C., Tortorici, E., Migdall, A. L., Zhang, Y., Kumor, D. R., Farr, W. H., Marsili, F., Shaw, M. D., Stern, J. A., Abellán, C., Amaya, W., Pruneri, V., Jennewein, T., Mitchell, M. W., Kwiat, P. G., Bienfang, J. C., Mirin, R. P., Knill, E., and Nam, S. W., "Strong Loophole-Free Test of Local Realism*," *Physical Review Letters* **115**, 250402 (Dec. 2015).

[21] Peacock, A., Verhoeve, P., Rando, N., van Dordrecht, A., Taylor, B. G., Erd, C., Perryman, M. A. C., Venn, R., Howlett, J., Goldie, D. J., Lumley, J., and Wallis, M., "Single optical photon detection with a superconducting tunnel junction," *Nature* **381**, 135–137 (May 1996).

[22] Bergman, A. S., Ade, P. A. R., Akers, S., Amiri, M., Austermann, J. A., Beall, J. A., Becker, D. T., Benton, S. J., Bock, J. J., Bond, J. R., Bryan, S. A., Chiang, H. C., Contaldi, C. R., Domagalski, R. S., Doré, O., Duff, S. M., Duivenvoorden, A. J., Eriksen, H. K., Farhang, M., Filippini, J. P., Fissel, L. M., Fraisse, A. A., Freese, K., Galloway, M., Gambrel, A. E., Gandilo, N. N., Ganga, K., Grigorian, A., Gualtieri, R., Gudmundsson, J. E., Halpern, M., Hartley, J., Hasselfield, M., Hilton, G., Holmes, W., Hristov, V. V., Huang, Z., Hubmayr, J., Irwin, K. D., Jones, W. C., Khan, A., Kuo, C. L., Kermish, Z. D., Li, S., Mason, P. V., Megerian, K., Moncelsi, L., Morford, T. A., Nagy, J. M., Netterfield, C. B., Nolta, M., Osherson, B., Padilla, I. L., Racine, B., Rahlin, A. S., Redmond, S., Reintsema, C., Romualdez, L. J., Ruhl, J. E., Runyan, M. C., Ruud, T. M., Shariff, J. A., Shaw, E. C., Shiu, C., Soler, J. D., Song, X., Trangsrud, A.,

Tucker, C., Tucker, R. S., Turner, A. D., Ullom, J., van der List, J. F., Van Lanen, J., Vissers, M. R., Weber, A. C., Wehus, I. K., Wen, S., Wiebe, D. V., and Young, E. Y., "280 GHz Focal Plane Unit Design and Characterization for the SPIDER-2 Suborbital Polarimeter," *ArXiv e-prints* (Nov. 2017).

[23] Hui, H., Ade, P. A. R., Ahmed, Z., Alexander, K. D., Amiri, M., Barkats, D., Benton, S. J., Bischoff, C. A., Bock, J. J., Boenish, H., Bowens-Rubin, R., Bowens-Rubin, R., Buder, I., Bullock, E., Buza, V., Connors, J., Filippini, J. P., Fliescher, S., Grayson, J. A., Halpern, M., Harrison, S., Hilton, G. C., Hristov, V. V., Irwin, K. D., Kang, J., Karkare, K. S., Karpel, E., Kefeli, S., Kernasovskiy, S. A., Kovac, J. M., Kuo, C. L., Leitch, E. M., Lueker, M., Megerian, K. G., Monticue, V., Namikawa, T., Netterfield, C. B., Nguyen, H. T., O'Brient, R., Ogburn, R. W., Pryke, C., Reintsema, C. D., Richter, S., Schwarz, R., Sorensen, C., Sheehy, C. D., Staniszewski, Z. K., Steinbach, B., Teply, G. P., Thompson, K. L., Tolan, J. E., Tucker, C., Turner, A. D., Vieregg, A. G., Wandui, A., Weber, A. C., Wiebe, D. V., Willmert, J., Wu, W. L. K., and Yoon, K. W., "BICEP3 focal plane design and detector performance," in [*Millimeter, Submillimeter, and Far-Infrared Detectors and Instrumentation for Astronomy VIII*], *Proc. SPIE* **9914**, 99140T (July 2016).

[24] The EBEX Collaboration, Abitbol, M., Aboobaker, A. M., Ade, P., Araujo, D., Aubin, F., Baccigalupi, C., Bao, C., Chapman, D., Didier, J., Dobbs, M., Feeney, S. M., Geach, C., Grainger, W., Hanany, S., Helson, K., Hillbrand, S., Hilton, G., Hubmayr, J., Irwin, K., Jaffe, A., Johnson, B., Jones, T., Klein, J., Korotkov, A., Lee, A., Levinson, L., Limon, M., MacDermid, K., Miller, A. D., Milligan, M., Raach, K., Reichborn-Kjennerud, B., Reintsema, C., Sagiv, I., Smecher, G., Tucker, G. S., Westbrook, B., Young, K., and Zilic, K., "The EBEX Balloon Borne Experiment - Detectors and Readout," *ArXiv e-prints* (Mar. 2018).

[25] Fixsen, D. J., Moseley, S. H., Gerrits, T., Lita, A. E., and Nam, S. W., "Optimal Energy Measurement in Nonlinear Systems: An Application of Differential Geometry," *Journal of Low Temperature Physics* **176**, 16–26 (July 2014).

[26] Irwin, K. D. and Hilton, G. C., "Transition-edge sensors," in [*Topics in Applied Physics: Cryogenic Particle Detection*], Enss, C., ed., Springer, Berlin (2005).

[27] Roberge, A., Arney, G. N., and Domagal-Goldman, S. D. Private communication (2018).

[28] Busch, S. E., Adams, J. S., Bandler, S. R., Chervenak, J. A., Eckart, M. E., Finkbeiner, F. M., Fixsen, D. J., Kelley, R. L., Kilbourne, C. A., Lee, S.-J., Moseley, S. H., Porst, J.-P., Porter, F. S., Sadleir, J. E., and Smith, S. J., "Progress Towards Improved Analysis of TES X-ray Data Using Principal Component Analysis," *Journal of Low Temperature Physics* **184**, 382–388 (July 2016).